*Quantum Electronics* **52** (5) 449–453 (2022) 

https://doi.org/10.1070/QEL18041

# Specific features of radiation flux formation in diode-pumped lasers and amplifiers with active elements made of Nd:YAG ceramics

M.V. Bogdanovich, V.N. Dudikov, K.V. Lepchenkov, V.A. Loiko, Yu.M. Popov, A.G. Ryabtsev, G.I. Ryabtsev, P.V. Shpak, M.A. Shchemelev

*Abstract.* **The spatial, temporal, and spectral characteristics of the output radiation of diode-pumped laser systems and optical amplifiers with active elements made of Nd:YAG ceramics are studied. It is shown that the divergence of radiation in the subthreshold regime has the form of concentric nested cones emerging from the active element (AE) faces at angles of 2–4°. A model explaining the experimentally observed phenomenon is proposed based on the mechanism of scattering of the generated beam from the granular structure of the optical ceramics. Analysis of the divergence pattern makes it possible to estimate the grain size and the optical quality of ceramics. The output beam divergence in the lasing regime is determined mainly by the cavity parameters and does not exceed several milliradians. The scattering events in this case serve as sources of additional optical losses. Luminescence enhancement and parasitic oscillations in the AE volume restrict the possibility of using Nd:YAG ceramics for fabricating AEs of high-power optical amplifiers.**

***Keywords:*** *Nd:YAG ceramic laser system, optical amplifier, optical ceramics, transverse diode pumping, amplified luminescence, parasitic oscillations.*

## 1. Introduction

The optical parameters of active elements (AEs) made of Nd:YAG ceramics are being continuously improved [1–4], which rapidly extends the application fields of laser sources with ceramic AEs. The most attractive properties of Nd:YAG optical ceramics are the relatively low production cost and the possibility of fabricating active media with high concentrations of neodymium ions. However, the thermal and optical characteristics of Nd:YAG ceramics are somewhat different from those of Nd:YAG single crystal [5–7]. Therefore, it is important to reveal and study the specific features of operating characteristics of laser sources with ceramic AEs, especially in view of development of high-power diode-pumped optical systems.

The present work is devoted to the study of the conditions of the formation of radiation fluxes in ceramic Nd:YAG AEs transversely excited by arrays of high-power laser diodes. The spatial, temporal, and spectral characteristics of sources (lasers and systems with optical amplifiers) with ceramic AEs are analysed in the free-running and *Q*-switched regimes, as well as in the amplified luminescence regime. The possibility of a correlation between the output beam optical parameters and the internal granular structure of the ceramic active medium is discussed.

## 2. Experiment

The mutual positions of the main element used in the experimental investigations of emitters with ceramic Nd:YAG AEs, as well as the near- and far-field radiation patterns, are presented in Fig. 1. We studied cylindrical AEs with diameters of 7 and 8 mm, which were made of Nd:YAG optical ceramics (Konoshima Chemical & Baikowski Japan Co.) with a neodymium ion concentration of 2 at %. The length of the AEs was 120 mm. The AE faces were antireflection coated for the wavelength $\lambda$ = 1.06 μm. The AEs were transversely pumped by three blocks of laser diode arrays (LDAs) arranged in three rows uniformly along the AE. Each block included three SLM-3 LDAs (Inject, Russia) mounted so that they were radially symmetric with respect to the AE axis. To achieve the maximum homogeneity of the pump radiation distribution in the AE volume, the LDAs of each block were rotated at an angle of 40° with respect to the position of arrays of the neighbouring block, as illustrated in Fig. 1. The LDAs were excited by rectangular current pulses with a duration of 170 μs and a repetition rate $f$ = 1–100 Hz. The experiments with the laser system were performed at $f$ = 10 Hz in the amplified luminescence regime (without an output mirror) and at $f$ from 1 to 100 Hz in the lasing regime. The pulse energy of an individual LDA was maintained at a level of ~260 mJ during all measurements at room temperature. The total pump pulse energy for each AE was 2.34 J. The pump band peak was tuned to $\lambda$ = 810.10 nm using an automatic LDA temperature control system based on Peltier elements.

**M.V. Bogdanovich, V.N. Dudikov, K.V. Lepchenkov, V.A. Loiko, A.G. Ryabtsev, G.I. Ryabtsev, P.V. Shpak, M.A. Shchemelev**
B.I. Stepanov Institute of Physics, National Academy of Sciences of Belarus, prosp. Nezavisimosti 68-2, 220072 Minsk, Belarus;
e-mail: ryabtsev@dragon.bas-net.by, m.bogdanovich@ifanbel.bas-net.by, dudikov.vn@gmail.com, k.lepchenkov@gmail.com, loiko@ifanbel.bas-net.by, p.shpak@dragon.bas-net.by, p.shpak@dragon.bas-net.by;
**Yu.M. Popov** P.N. Lebedev Physical Institute of the Russian Academy of Sciences, Leninsky prosp. 53, 119991 Moscow, Russia;
e-mail: popovym@lebedev.ru

Received 12 December 2021; revision received 10 March 2022
*Kvantovaya Elektronika* **52** (5) 449–453 (2022)
Translated by M.N. Basieva

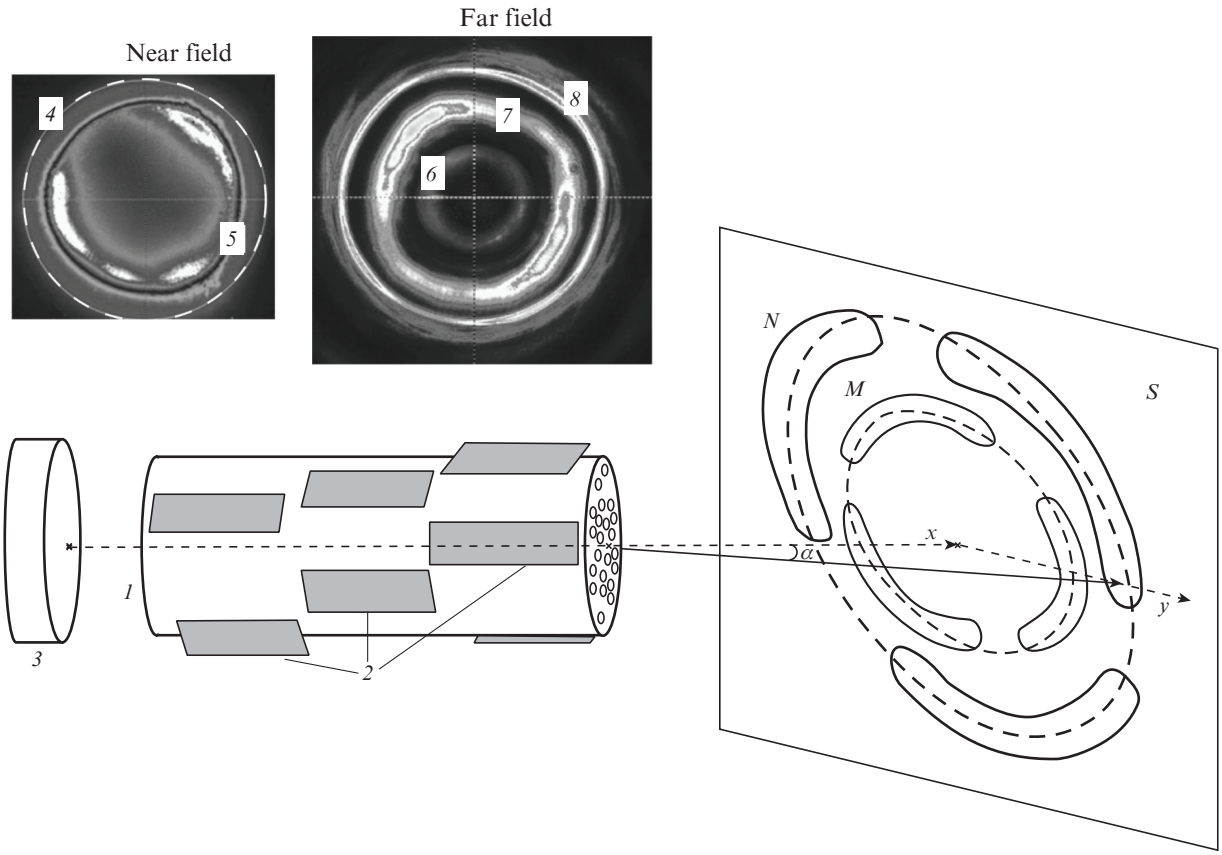


**Figure 1.** Scheme of experiments with a Nd:YAG source:
(*1*) AE made of optical ceramics; (*2*) three rows of pumping LDA blocks; (*3*) highly reflecting rear mirror ($\lambda$ = 1.06 μm); (*4*) limiting contour of the photorecording system; (*5*) near-field aperture of the output radiation; (*6*, *7*, *8*) rings of the far-field pattern of radiation emitted from the AE face. Plane *S* shows the far-field pattern obtained by scanning of a small-aperture photodetector in the plane perpendicular to the *x* axis; annular structure *M* corresponds to the intensity distribution at $\alpha_1 \approx 2.75°$; annular structure *N* is the intensity distribution at $\alpha_2 \approx 4°$.

## 3. Ceramic AE in a nonlasing regime

At the initial stage of experiments, rear mirror *3* (Fig. 1) was removed and we analysed the spatial distribution of radiation intensity emitted from the AE face in the near-field (at a distance of less than 1 cm from the AE face) and far-field approximations. The far-field pattern was recorded by scanning a small-aperture photodetector in the *S* plane, which is perpendicular to the *x* axis and spaced by 40 cm from the AE face. In addition to this procedure, the far-field pattern was photographed using an IR camera.

Analysis of the near- and for-field patterns shown in Fig. 1 allows us to conclude that the radiation emitted from the face of the AE of the Nd:YAG emitter operating in a nonlasing regime has the form of two or more beams propagating along nested coaxial conical surfaces. The typical dependence of the output intensity $I$ on the divergence angle $\alpha$ is presented in Fig. 2a. The low-intensity maximum of the $I(\alpha)$ dependence at $\alpha_1 \approx 2.75°$ is related to the ring structure *M*, and the more intense maximum at $\alpha_2 \approx 4°$ belongs to the ring structure *N* on plane *S*.

The dependences of intensity $I$ on the pump pulse evolution time $t$ observed at angles $\alpha_1$ and $\alpha_2$ are different (Fig. 2b). Curve (*1*) corresponds to the dependence $I(t)$ for radiation emitted from the AE face along the *x* axis ($\alpha = 0$), and curve (*2*) belongs to the beam propagating at an angle $\alpha = 4°$. Based on the parameters of the AE and the pump units, we analysed the shapes of curves (*1*) and (*2*) using the system of differential equations taking into account spontaneous emission, amplified luminescence, and parasitic off-axis modes [8–10]. It is found that curve (*1*) represents a $I(t)$ dependence typical for a Nd:YAG source operating in a nonlasing (subthreshold) regime and corresponds to spontaneous emission. Intensity $I$ in this case continuously increases to a maximum value for the time interval OE and then, at $t > 170$ μs, exponentially decreases to zero with the time constant $\tau_D \sim 120$–150 μs, which coincides in the order of magnitude with the fluorescence lifetime of ceramic Nd:YAG AEs with a neodymium concentration of 2 at % [3, 11–13]. Curve (*2*) represents a $I(t)$ dependence typical for a Nd:YAG emitter operating in the regime of spontaneous emission enhancement (amplified luminescence), which is studied in sufficient detail in [8–10]. This regime is characterised by a superlinear increase in the output radiation intensity during the pump pulse action (interval OE in Fig. 2b) and by a sharp decrease in intensity after the pulse termination. Curve (*2*) in the range of its sharp decline ($t > 170$ μs) is approximated by three constants $\tau_D$ equal to 28, 80, and 109 μs. At $t > 300$–320 μs, the $I(t)$ dependence declines with the time constant $\tau_D \approx 120$–150 μs.

The spectral characteristics of radiation beams exiting the face of the Nd:YAG AE at different angles $\alpha$ are also different. For example, the spectral peak in the region of $\lambda$ = 1.06 μm, which belongs to the beam exiting the AE at an angle $\alpha_2 \approx 4°$, has a higher amplitude than the peak recorded at $\alpha = 0$ (Fig. 3).

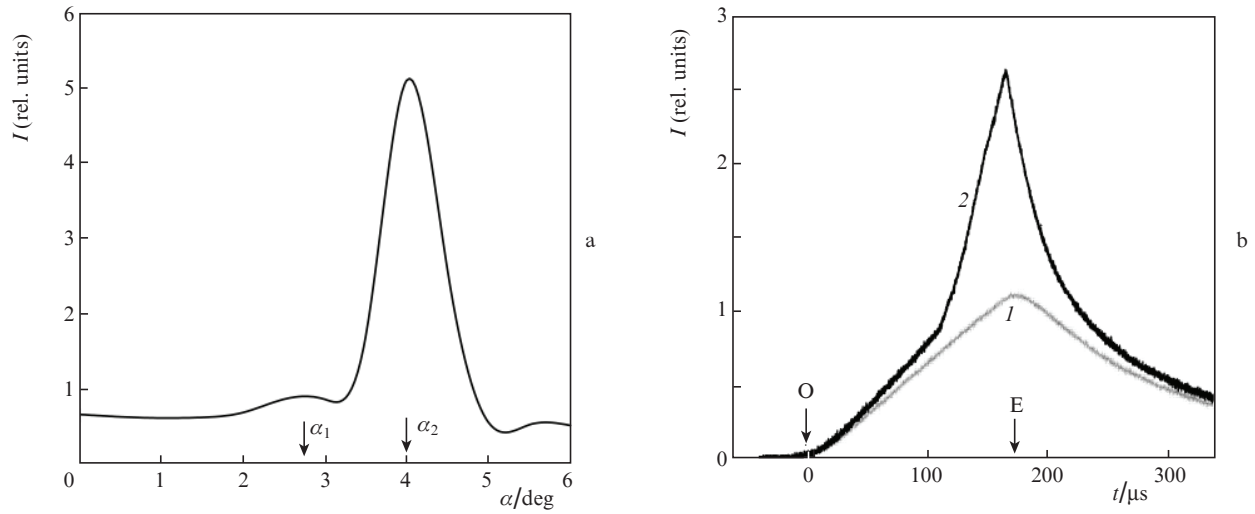


**Figure 2.** Dependences of radiation intensity $I$ on (a) the angle $\alpha$ and (b) the pulse development time $t$ for a Nd : YAG source in the nonlasing regime. Points O and E indicate the beginning and end of the pump pulse. The radiation is emitted from the AE face at angles $\alpha$ = (*1*) 0 and (*2*) 4°.

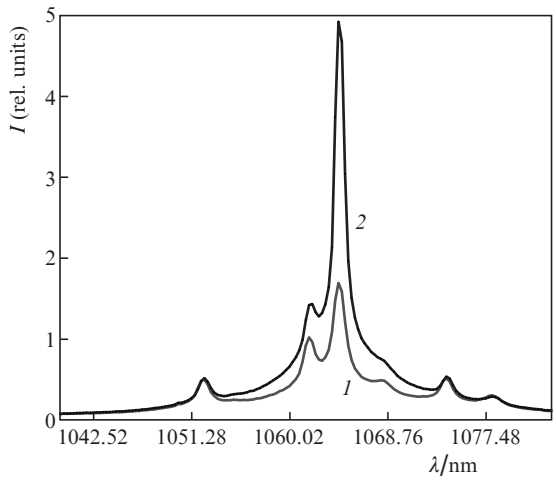


**Figure 3.** Spectra of radiation emitted from the face of the ceramic Nd : YAG AE in the nonlasing regime at angles $\alpha$ = (*1*) 0 and (*2*) 4°.

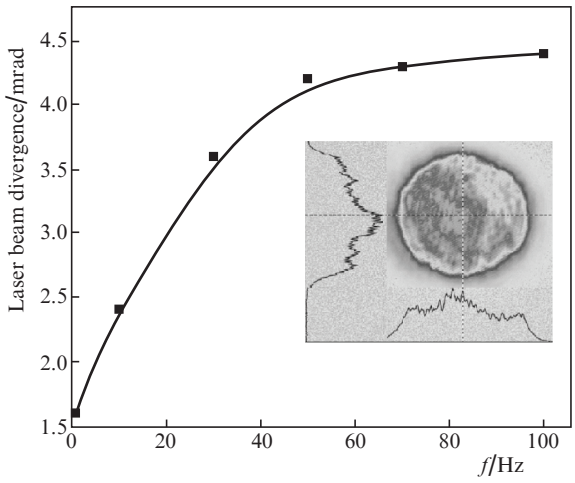


**Figure 4.** Dependence of the divergence of the output beam of the Nd : YAG laser with a ceramic AE in the free-running mode on the pulse repetition rate. The inset shows the far-field radiation pattern at $f$ = 70 Hz.

## 4. Laser source with an AE made of Nd : YAG ceramics

The specific features of the emission formation in ceramic AEs were also studied for Nd : YAG lasers and optical amplifiers. To this end, we placed an output mirror (not shown in Fig. 1) with a reflection coefficient of 50% for $\lambda$ = 1.06 μm to the right of the AE. The geometrical length of the optical cavity was 1.0 m. In the free-running regime, the laser emitted pulses with an energy of ~1 J. As the pulse repetition rate $f$ varied within the range 1–100 Hz, the pulse energy varied by no more than 5%. The laser beam divergence gradually increased from 1.6 to 4.4 mrad with $f$ increasing from 1 to 100 Hz (Fig. 4).

In the free-running regime of the Nd:YAG laser, the far-field intensity distribution of the beams propagating along the nested conical surfaces at angles of 2.0–2.5° and 4.0° remains the same, but the relative brightness of these beams considerably decreases on the background of the central spot of radiation propagating within a solid angle of several milliradians.

The ceramic Nd:YAG AE was also studied in the composition of an optical amplifier (OA) (Fig. 5a). In these experiments, the master laser pulses with a duration of ~10 ns, an energy of 0.12 J, and a Gaussian intensity profile were coupled into the cylindrical (diameter 8 mm, length 120 mm) ceramic AE of the optical amplifier. From Fig. 5b, one can see that the output pulse energy $E_{rad}$ in the case of a single-pass scheme almost linearly increases as the energy $E_p$ of pulses pumping the AE of the optical amplifier increases up to the maximum value $E_p \approx 2.5$ J. The amplifier output beam was 7 mm in diameter and had a divergence of several milliradians. The cross section of this beam is schematically shown in Fig. 5a as a black circle surrounded by a low-intensity ring structure formed by beams propagating along the nested coaxial conical surfaces and emitted from the AE face at angles $\alpha \sim 4°$.

For double-pass amplification, we placed a highly reflecting mirror in front of the output face of the AE (to the right

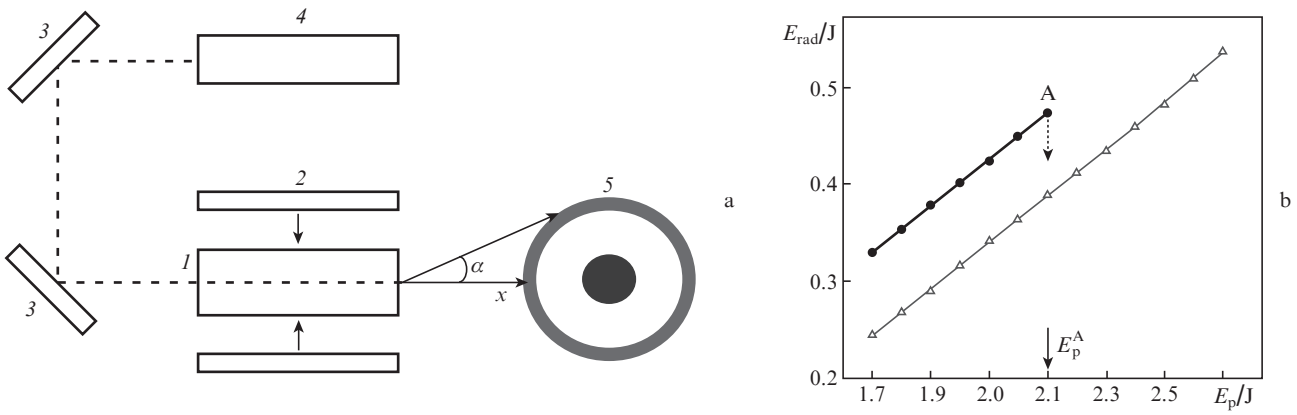


**Figure 5.** (a) Optical scheme of a single-pass laser amplifier:
(*1*) AE; (*2*) LDA; (*3*) folding mirrors; (*4*) master laser; (*5*) intensity distribution in the cross section of the output amplifier beam and (b) dependences of the optical amplifier output energy $E_{rad}$ (input pulse energy 0.12 J, $f = 10$ Hz) on the pump pulse energy $E_p$ for (▵) single- and (●) double-pass amplification schemes.

of the AE in Fig. 5a) and a $\lambda/4$ phase plate with a polarising cube in front of the input AE face (to the left of the AE in Fig. 5a). After reflection from the highly reflecting mirror and the second pass through the ceramic AE, the radiation was coupled out through the polarising cube perpendicular to the $x$ axis. After the second pass of the driving pulse through the AE of the optical amplifier, the $E_{rad}$ energy increased approximately by 1.3 times. In this case, similar to the case of the single-pass scheme, the $E_{rad}(E_p)$ function is approximated by a direct proportional dependence. At relatively low pump levels (1.7–1.8 J), the beam cross section recorded at the exit from the optical amplifier consisted of a central spot corresponding to the intense low-divergence beam ~7 mm in diameter and a surrounding ring of a larger diameter, which is similar to the intensity distribution (*5*) shown in Fig. 5a. However, further increase in $E_p$ leads to a fast increase in the peripheral ring intensity, because of which the energy of amplified pulses sharply decreases at $E_p^A \geqslant 2.1$ J (point A in Fig. 5b). The $I(t)$ dependence takes the form typical for amplified luminescence and/or parasitic oscillations [see, for example, curve (*2*) in Fig. 2], and the emission spectrum exhibits a narrow intense peak similar to peak *2* in Fig. 3.

The annular divergence pattern was also observed in the case of propagation of a collimated beam of a helium–neon laser through the ceramic AE along the $x$ axis.

## 5. Discussion of results

The obtained experimental results are explained as follows. The optical ceramic volume represents a densely packed polydisperse granular structure [1, 2, 4, 14]. The grain boundaries, foreign inclusions (pores), secondary phases, and surface defects of grain boundaries are the inhomogeneities causing radiation scattering. The near-surface region of the AE faces is also inhomogeneous.

Based on the results of [7–9], we can suggest that a partial ordering in the positions of ceramic grains leads to interference of scattered waves, which results in the formation of the annular structure of radiation emitted by the AE in the nonlasing regime (Fig. 6). According to the estimate made in [7–9] within the approach based on consideration of scattering processes in the near-surface region of the AE face, the grain size of the studied ceramics is 16 μm. To perform a more accurate analysis of the divergence pattern, it is necessary to take into account the contributions of scattering processes both in the near-surface regions of the AE and in its volume [10].

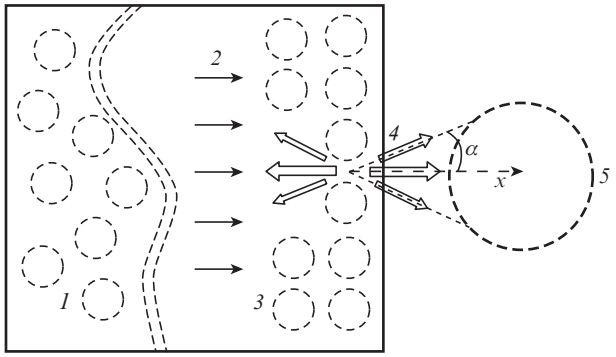


**Figure 6.** Schematic of radiation scattering in a ceramic Nd:YAG AE: (*1*) grains in the optical ceramics volume; (*2*) radiation flux; (*3*) grains in the near-surface AE layer; (*4*) scattered beams; (*5*) annular structure of the far-field output radiation.

The divergence pattern of the ceramic AE emission in the nonlasing regime is similar to the structure of coronas observed around bright stars, planets, the Sun, or the Moon as a result of light diffraction at water drops or ice crystals in clouds. The angular radii of coronas do not exceed 5° [15, 16], which is close to the angular radius (4°) of the main beam emitted from the ceramic AE. A rough estimate of Nd:YAG ceramics grains based on the diffraction formula for crystalline clouds [16] yields ~15 μm. It is important to note that, since the diffraction parameters correlate with the size of crystals, the width of the scattering ring (for example, in the region of angle $\alpha_2$) can be used to estimate the degree of grain size dispersion in the ceramic AE volume. The form of dependences of $I(\alpha)$, $I(t)$, and $I(\lambda)$ (see Figs 2, 3) allows us to suggest that the radiation emitted from the face of the ceramic Nd:YAG AE at angles $\alpha \sim 4°$ represents a flux of amplified luminescence and/or parasitic oscillations. In particular, curve (*2*) in Fig. 2 is a typical dependence of the intensity of

such a flux on the evolution time of the pulse pumping the Nd : YAG laser source [8–10], and the spectral maximum of this dependence coincides with gain maximum near $\lambda$ = 1.06 μm [curve (*2*) in Fig. 3]. The amplified luminescence and/or parasitic oscillations are formed in the process of radiation amplification during time intervals between multiple scattering events.

In the lasing regime, the radiation characteristics are determined mainly by the optical cavity parameters, because of which the output beam divergence does not exceed several milliradians. The scattering events in this case serve as sources of optical losses for the generated beam propagating along the laser cavity axis. An increase in these losses with increasing level of pumping of the optical amplifier is probably one of the reasons for a decrease in the energy of pulses amplified in the double-pass optical amplifier. At the instant when the output pulse energy $E_{rad}$ sharply decreases (point A in Fig. 5), the intensity of radiation emitted from the AE at angles $\alpha \sim 4°$ begins to increase, the $I(t)$ dependence and the narrow spectral line of this emission being typical for amplified luminescence and parasitic oscillations.

## 6. Conclusions

The spatial, temporal, and spectral characteristics of the output radiation of diode-pumped laser systems and optical amplifiers with AEs made of Nd : YAG ceramics are studied. It is shown that the radiation divergence in the subthreshold regime has the shape of concentric nested cones emitted from the AE face at angles of 2–4°. The dependences of the output radiation intensity on the pump pulse evolution time and on the wavelength recorded at different divergence angles (see Figs 2, 3) agree with those obtained in [8–10] studying the specific features of amplified luminescence and/or off-axis oscillations in solid-state AEs. This allows us to conclude that the radiation emitted from the face of the ceramic Nd : YAG AE at angles of ~4° is a flux of amplified luminescence and/or parasitic oscillations.

A model based on the mechanism of beam scattering by the granular structure of the optical ceramics is proposed to explain the experimentally observed divergence of the output radiation. Analysis of the divergence pattern makes it possible to estimate the grain size of the studied ceramics (15–16 μm) and its optical property.

It is shown that, in the lasing regime, radiation scattering from grains and structural defects of ceramics leads to amplified luminescence in the AE volume and/or to parasitic modes propagating at angles to the cavity axis and is an important source of optical losses. An increase in these losses with increasing pump intensity can be one of the factors limiting the application of Nd : YAG ceramics as an active medium of high-power lasers and optical amplifiers.

## References


1. Ikesue A., Aung Y.L., Taira T., Kamimura T., Yoshida K., Messing G.L. *Ann. Rev. Mater. Res.*, **36**, 397 (2006).
2. Li J., Wu Y., Pan Y., Liu W., Huang L., Guo J. *Opt. Mater.*, **31**, 6 (2008).
3. Bezotosnyi V.V., Balashov V.V., Bulaev V.D., Kaminskii A.A., Kanaev A.Yu., Kravchenko V.B., Kiselev A.V., Kopylov Yu.L., Koromyslov A.L., Krokhin O.N., Lopukhin K.V., Lysenko S.L., Pankov M.A., Polevov K.A., Popov Yu.M., Cheshev E.A., Tupitsyn I.M. *Quantum Electron.*, **48**, 802 (2018) [*Kvantovaya Elektron.*, **48**, 802 (2018)].
4. Ikesue A., Aung Y.L. *IEEE J. Sel. Top. Quantum Electron.*, **24**, 1601507 (2018).
5. Mukhin I.B., Palashov O.V., Khazanov E.A. *Opt. Express*, **13**, 5983 (2005).
6. Kim D.L., Kim B.T. *Optik*, **127**, 9738 (2016).
7. Ryabtsev G.I., Bogdanovich M.V., Grigor'ev A.V., Dudikov V.N., Lepchenkov K.V., Ryabtsev A.G., Shpak P.V., Shchemelev M.A. *Opt. Zh.*, **87**, 50 (2020).
8. Bezyazychnaya T.V., Bogdanovich M.V., Grigor'ev A.V., Kabanov V.V., Kostik O.E., Lebiadok Y.V., Lepchenkov K.V., Ryabtsev A.G., Ryabtsev G.I., Shchemelev M.A., Teplyashin L.L. *Opt. Commun.*, **308**, 26 (2013).
9. Bogdanovich M.V., Grigor'ev A.V., Lantsov K.I., Lebedok E.V., Lepchenkov K.V., Ryabtsev A.G., Ryabtsev G.I., Shchemelev M.A. *J. Appl. Spectrosc.*, **82**, 537 (2015) [*Zh. Prikl. Spectrosk.*, **82**, 538 (2015)].
10. Bogdanovich M.V., Grigor'ev A.V., Ryabtsev A.G., Ryabtsev G.I., Shpak P.V., Shchemelev M.A., Lepchenkov K.V., Lantsov K.I., Dudikov V.N., Kot A.M. *Opt. Zh.*, **85**, 31 (2018).
11. Ikesue A., Kamata K., Yoshida K. *J. Am. Ceram. Soc.*, **76**, 1921 (1996).
12. Lu J., Prabhu M., Song J., Li C., Xu J., Ueda K., Kaminskii A.A., Yagi H., Yanagitani T. *Appl. Phys. B*, **71**, 469 (2000).
13. Yagi H., Yanagitani T., Takaichi K., Ueda K., Kaminski A. *Opt. Mater.*, **29**, 1258 (2007).
14. Vorona I.O., Avetskii R.P., Shpilinskaya O.L., Kos'yanov D.Yu., Doroshenko A.G., Parkhomenko S.V., Lopin A.V., Tolmachev A.V. *Tech. Phys. Lett.*, **41**, 456 (2015) [*Pis'ma Zh. Tekh. Phys.*, **41**, 72 (2015)].
15. Sivukhin D.V. *Obshchii kurs fiziki. Optika* (General Course of Physics. Optics) (Moscow: Nauka, 1980).
16. Zvereva S.V. *V mire solnechnogo sveta* (In the World of Sunshine) (Leningrad: Gidrometeoizdat, 1988).